



Fast SARS-CoV-2 virus detection using disposable cartridge strips and a semiconductor-based biosensor platform ^F

Cite as: J. Vac. Sci. Technol. B **39**, 033202 (2021); <https://doi.org/10.1116/6.0001060>

Submitted: 29 March 2021 . Accepted: 26 April 2021 . Published Online: 18 May 2021

Minghan Xian, Hao Luo, Xinyi Xia,  Chaker Fares,  Patrick H. Carey, Chan-Wen Chiu,  Fan Ren, Siang-Sin Shan, Yu-Te Liao, Shu-Min Hsu,  Josephine F. Esquivel-Upshaw, Chin-Wei Chang, Jenshan Lin, Steven C. Ghivizzani, and  Stephen J. Pearton

COLLECTIONS

 This paper was selected as Featured



View Online



Export Citation



CrossMark



Advance your science and
career as a member of

AVS

LEARN MORE








Fast SARS-CoV-2 virus detection using disposable cartridge strips and a semiconductor-based biosensor platform

Cite as: J. Vac. Sci. Technol. B 39, 033202 (2021); doi: 10.1116/6.0001060

Submitted: 29 March 2021 · Accepted: 26 April 2021 ·

Published Online: 18 May 2021



Minghan Xian,^{1,a)} Hao Luo,¹ Xinyi Xia,¹ Chaker Fares,¹  Patrick H. Carey IV,¹  Chan-Wen Chiu,¹ Fan Ren,¹  Siang-Sin Shan,² Yu-Te Liao,² Shu-Min Hsu,³ Josephine F. Esquivel-Upshaw,³  Chin-Wei Chang,⁴ Jenshan Lin,⁴ Steven C. Ghivizzani,⁵ and Stephen J. Pearton⁶ 

AFFILIATIONS

¹Department of Chemical Engineering, University of Florida, Gainesville, Florida 32611

²Department of Electrical and Computer Engineering, National Chiao Tung University, Hsinchu 30010, Taiwan

³Department of Restorative Dental Sciences, University of Florida, Gainesville, Florida 32610

⁴Department of Electrical and Computer Engineering, University of Florida, Gainesville, Florida 32611

⁵Department of Orthopaedics and Rehabilitation, University of Florida, Gainesville, Florida 32610

⁶Department of Materials Science and Engineering, University of Florida, Gainesville, Florida 32611

^{a)}Electronic mail: mxian@ufl.edu

ABSTRACT

Detection of the SARS-CoV-2 spike protein and inactivated virus was achieved using disposable and biofunctionalized functional strips, which can be connected externally to a reusable printed circuit board for signal amplification with an embedded metal–oxide–semiconductor field-effect transistor (MOSFET). A series of chemical reactions was performed to immobilize both a monoclonal antibody and a polyclonal antibody onto the Au-plated electrode used as the sensing surface. An important step in the biofunctionalization, namely, the formation of Au-plated clusters on the sensor strips, was verified by scanning electron microscopy, as well as electrical measurements, to confirm successful binding of thiol groups on this Au surface. The functionalized sensor was externally connected to the gate electrode of the MOSFET, and synchronous pulses were applied to both the sensing strip and the drain contact of the MOSFET. The resulting changes in the dynamics of drain waveforms were converted into analog voltages and digital readouts, which correlate with the concentration of proteins and virus present in the tested solution. A broad range of protein concentrations from 1 fg/ml to 10 µg/ml and virus concentrations from 100 to 2500 PFU/ml were detectable for the sensor functionalized with both antibodies. The results show the potential of this approach for the development of a portable, low-cost, and disposable cartridge sensor system for point-of-care detection of viral diseases.

Published under an exclusive license by the AVS. <https://doi.org/10.1116/6.0001060>

INTRODUCTION

The outbreak of the highly infectious SARS-CoV-2 virus (COVID-19) has led to a global pandemic, mainly through the spread of respiratory droplets during in-person gatherings. Public health practices such as home quarantine, social distancing, disinfection, and the use of personal protection equipment (PPE) remain as the main preventive approaches.¹ According to the World Health Organization (WHO), as of late March 2021, there have been over 125×10^6 confirmed cases globally, with over 2.7×10^6 deaths.² Although vaccination on a massive scale and

research into potential therapeutics are underway, rapid testing and diagnostics for COVID-19 are still needed for safe resumption of daily activity. Presently, there are two main methods of detection for the diagnosis of COVID-19. The reverse transcription polymerase chain reaction (RT-PCR) method is the most widely used direct test for the presence of SARS-CoV-2 virus,^{3–5} with antibody tests used as a supplemental tool. Serology tests require longer times compared with PCR; however, tests such as Enzyme-Linked Immunosorbent Assays (ELISA) and chemiluminescence are able to scale to large throughput and bring a reduction in cost and

test-to-result time, according to Marca *et al.*⁵ The spiked protein is crucial for the binding and fusion of the virus, where the S1 protein is responsible for binding, while the S2 protein is responsible for fusion.^{6,7} Numerous sensing technologies have also been established that are based on the receptor binding domain of S proteins for human coronaviruses.^{5,8–12}

Aside from collection through conventional oropharyngeal and nasopharyngeal swabs, SARS-CoV-2 has also been detected in human saliva, which indicates that this may contribute as a route of transmission, but also provides an opportunity for virus testing with a noninvasive and facile method of collection.^{4,13–20} In fact, Wyllie *et al.* compared patient-match saliva and nasopharyngeal samples and concluded that saliva tests yield increased titer detection, reduced variability, and improved consistency in RT-PCR.¹⁴ Also, the self-collection method is noninvasive, and it also minimizes the interaction between patient and healthcare workers while requiring no specialized transport medium.¹⁵ These appealing features make saliva an appealing platform for adaptation in diagnostic tools.

Electrochemical-based biosensor systems are one example of serology tests for COVID-19 that utilizes the formation of an antigen–antibody complex on a sensing surface to perform diagnosis.⁹ A number of such sensors have been previously demonstrated using various materials of construction and sensing technologies.⁹ Seo *et al.* utilized graphene-based field-effect transistors (FETs) to demonstrate the detection of the spike protein in cultured virus and clinical samples for SARS-CoV-2.⁸ An electrochemical impedance-based detector for the SARS-CoV-2 antibody has been demonstrated by Rashed *et al.*,¹² while Alafeef *et al.* have successfully functionalized antisense oligonucleotides on sensor surfaces for nucleocapsid protein sensing.²¹

Regardless of the target for sensing and the material of construction, the cost of manufacturing/testing and ease of transportation are key for successful commercialization of a sensor system. Similar to many other transistor technologies, AlGaIn/GaN high-electron mobility transistors (HEMTs) have been studied extensively for the detection of various chemicals and biomarkers;^{22–26} however, the gate of these transistors is exposed as the sensing surface, which makes the cost of replacing the sensor prohibitive for large-scale use. A much less costly approach is the detection of the biomarker using a disposable sensor fabricated on glass slides. This has been used previously to detect cerebrospinal fluid (CSF), cardiac troponin I, and Zika virus, using a synchronous double-pulsed bias voltage on both the gate and the drain of the transistor and an externalized MOSFET.^{10,27–31}

In this work, a modular biosensor system consisting of a Si-MOSFET with a built-in digital readout is demonstrated, in combination with externalized cartridge sensor strips, for fast detection of the COVID-19 S protein as well as human-inactivated virus in a saliva platform.

MATERIAL AND METHOD

Commercially available glucose test strips were used as bio-functionalized cartridges for electrochemical measurements. The general schematic of the system is shown in Fig. 1(a). The carbon electrodes within the microfluidic channel of the test strip were gold-plated using a gold-plating solution, and biofunctionalized

with SARS-CoV-2 antibodies; meanwhile, the middle electrode was electrically connected to the gate electrode of the MOSFET (Texas Instruments SN74S124N). The Au-plated electrodes within the microfluidic channel were first treated with 10 mM thioglycolic acid (TGA) in ethanol for 4 h. The formation of Au–S bonding was verified by electrical measurement and x-ray photoelectron spectroscopy, as done in previous work.^{22,23} To validate the successful formation of Au–S bonding using such a method, electrical measurement was made using an Agilent 4156C parameter analyzer to measure the current between an Au-plated carbon electrode treated with ethanethiol (EtSH) and an auxiliary nonplated carbon electrode. The current was observed to decrease significantly with increasing the treatment time and EtSH concentration, indicating coverage of the surface by the functional layer.

Subsequently, a two-step chemical reaction was used to enhance the antibody binding via submerging the TGA functionalized electrode in N,N'-dicyclohexylcarbodi-imide (0.1 mM) in acetonitrile for 30 min and N-hydroxysuccinimide (0.1 mM) in acetonitrile for an hour. Excess reactant was rinsed off with acetonitrile and DI wafer after the reaction. Two different types of SARS-CoV-2 (COVID-19) antibody, MCA-5G8 monoclonal antibody (EnCor Biotechnology) and polyclonal spike antibody (Prosci #3535), were used to functionalize test strips. 20 µg/ml of antibody solution in phosphate buffer solution (PBS) was introduced to the electrode surface and was incubated for 18 h at 4 °C. Then, the test strips were rinsed with PBS and stored in a refrigerator at 4 °C before use. Both SARS-CoV-2 spike peptide (Prosci 3525P) and inactivated virus (ATCC VR-1986HK) were diluted serially in saliva and were stored at 4 °C before use.

A printed circuit board (PCB), Fig. 1(b), was designed to send a synchronous voltage pulse signal to both the gate and drain electrodes of the MOSFET, using the double-pulse method developed previously.^{22–26} The drain pulse duration (square wave at V_{DD}) was around 1.1 ms at a constant voltage, whereas the gate pulse started at around 40 µs after the onset of the drain pulse signal and stopped at 40 µs before the end of the drain pulse. A 13 kΩ resistor was connected to the drain as a load resistor, shown in Fig. 1(c). The circuit board was able to generate pulse signals and convert the analog drain output of the MOSFET into a four-digit digital output after each pulse trigger. Analog drain waveform (V_D) was collected using an Agilent InfiniiVision DSO7054B oscilloscope, and voltage reading at 750 µs was extracted as the analog reading. A voltage-controlled oscillator (SN74S124 N) was used to convert the drain waveform into a frequency output, and it was subsequently integrated by using a built-in Arduino microcontroller to translate into a four-digit digital signal, shown in Fig. 1(c). A built-in LCD screen was used for displaying the result. Eight pulse signals were collected and averaged for each sampling concentration for the analog signal and digital readout.

RESULT AND DISCUSSION

To prepare a sensing surface immobilized with the proper antibody of choice for electrical measurement, a metal surface made with Au or Ag is required to initiate the sequence of reaction chemistry for surface biofunctionalization.^{32–34} The SEM images, Fig. 2, show the time-dependent evolution of coverage of the plated

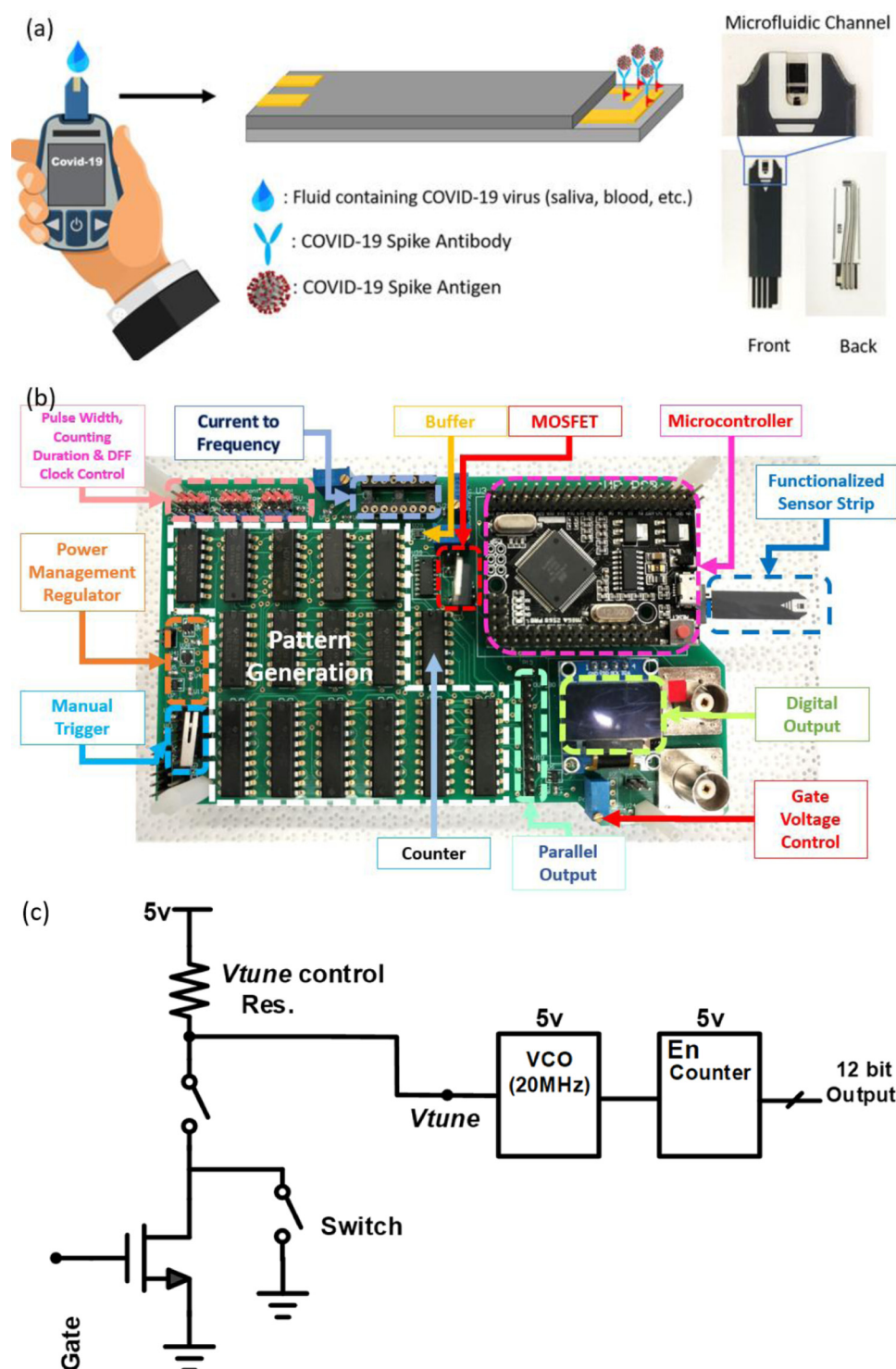


FIG. 1. Schematics and photograph of the sensor strip used in measurement (a), printed circuit board fabricated to produce digital sensor output with a built-in microcontroller (b) and architecture of a digital signal generation mechanism (c).

gold clusters on the carbon electrodes. A rapid onset of nucleation occurs within the first minute of plating, and the particle size continues to grow and form agglomerates during the remainder of the process. Particle growth results in spikes and shards on this cluster

surface, but no further nucleation of particles is observed after 1.5 min. To further increase the surface area, functionalization using nanoscale Au particles can be considered in the future instead of electroplating.

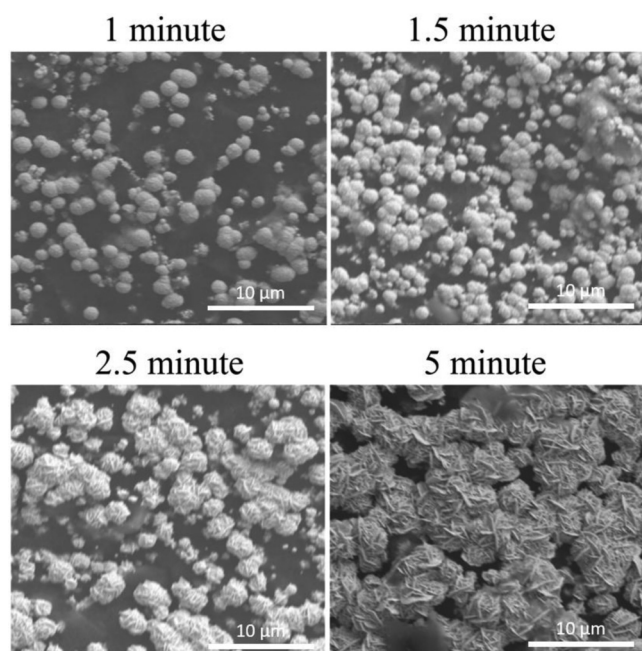


FIG. 2. SEM images of gold clusters formed on a graphite surface within a microfluidic channel at different plating times.

An additional study was performed to examine the reaction kinetics of the Au-S bond formation, as one of the most vital parts in the biofunctionalization on top of the Au-plated carbon electrode. EtSH was used as a surrogate of (TGA) to study the process of formation of the self-assembled Au-S monolayer.^{22,23} The hydrophobic end of EtSH faces toward the solution and gradually forms an insulating layer from ions within the solution, and eventually become electrically insulating. Figure 3(a) shows the time-dependent current-voltage (*I*-*V*) characteristics from 0 to 0.3 V, as 10 mM of EtSH solution in PBS was applied onto the Au-plated electrode surface. A rapid reduction in current was observed within a 15 min time frame and above 97% coverage was indicated from the electrical measurement. Figure 3(b) shows the surface coverage percentage as a function of time and as a function of EtSH concentration. The facile kinetics enables fast formation of the surface self-assembled layer, with above 90% coverage within 15 min even for EtSH concentrations below 10 mM. For an actual test strip functionalized with the COVID antibody, the Au electrodes were immersed within the 10 mM TGA solution for 12 h, providing sufficient time for surface coverage.

The time-dependent drain waveforms are shown in Fig. 4 at concentrations ranging from 1 fg/ml to 10 μg/ml. For comparison across different concentrations, the drain voltage levels at fixed 750 μs were extracted from each curve and compared in Figs. 5(a) and 6(a) for the spike protein and heat-inactivated virus, respectively. Note that the dynamic behavior of the drain waveform was dependent on the absolute value of resistance of the load resistor between the V_{DD} and the drain electrode, as well as the dynamic

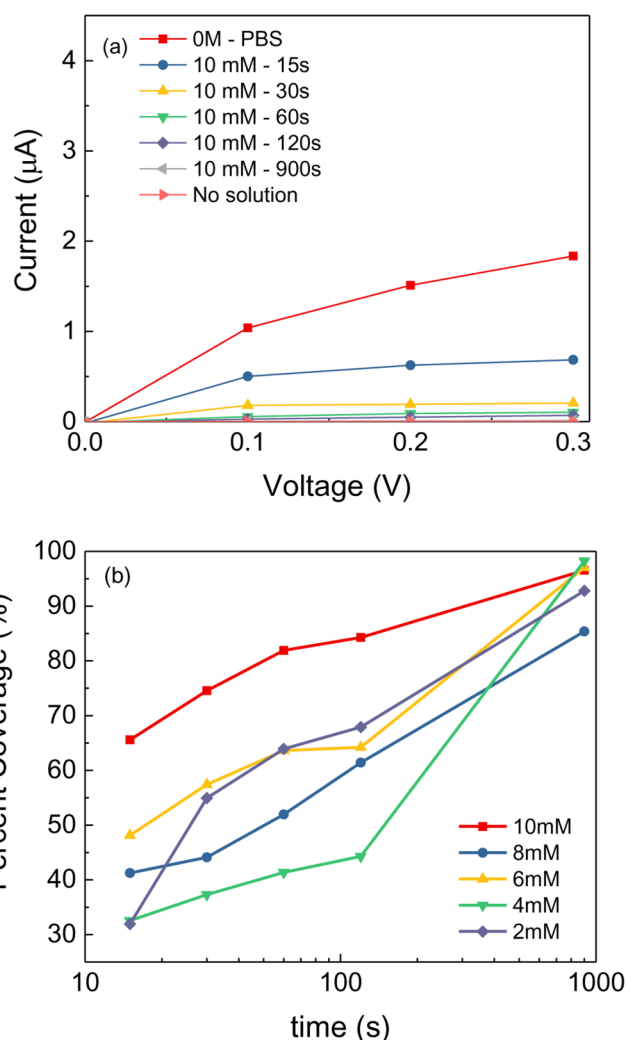


FIG. 3. Current-voltage characteristics of an Au-plated sensor strip reacting with 10 mM ethanethiol solution in PBS at different times (a) and coverage of ethanethiol on a gold surface converted by current measured 1 V as a function of concentration from 10 s to 15 min of reaction time (b).

behavior of protein on the sensing surface. As described and modeled previously, antigen-antibody complexes stretch and contract as a double springs under a pulsed gate electric field throughout a protein structure and cause the entire complex to move.³²⁻³⁴ This variation in protein structure leads to a time-dependent electric field applied to the gate of the MOSFET and produces a spring-like behavior in the drain voltage waveform, since the sensor strip is externally connected with the gate electrode of the MOSFET. In Fig. 5, it is seen that increasing the spike peptide concentration causes a consistent drop in the drain voltage, as well as a reduction in the converted digital reading. The measurement of the analog drain voltage was performed via measurement of the potential difference between the drain of the MOSFET and the source, where a

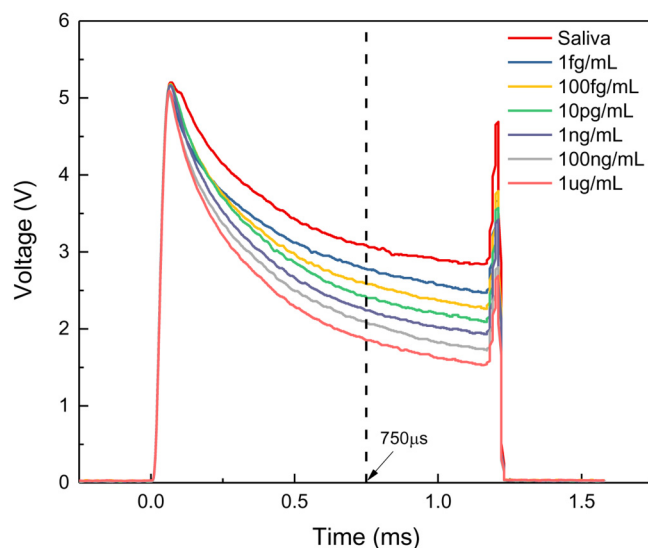


FIG. 4. Example MOSFET drain waveform at a fixed gate voltage (1.5 V) for different SARS-CoV-2 spike peptide concentrations in saliva using a test strip functionalized with a SARS-CoV-Spike antibody. The voltage of interest was extracted at $750\ \mu\text{s}$ from these waveforms.

reduction in drain voltage signifies an increase of conductance and elevated drain current. Improved smoothness of the data curve was achieved by averaging over eight consecutive and identical pulse measurements. The total measurement time was less than 10 ms, and, thus, this approach can provide real-time measurement for point-of-service applications.

For a range of spike protein concentrations from 0 g/ml up to $10\ \mu\text{g/ml}$ in saliva, Fig. 5(a) shows that the drain voltage extracted at $750\ \mu\text{s}$ of the drain waveform decreases monotonically for 1.31 V for the monoclonal antibody and 1.24 V for polyclonal antibody, both with a linear profile with a sensitivity of 117 mV/dec for the monoclonal antibody and 86 mV/dec for polyclonal antibody. This shows the large dynamic range and large signal output achieved for the tested peptide concentrations. Digital readings from the built-in LCD are shown in Fig. 5(b). There is a range of digital readout from 2584 to 3459 for the monoclonal antibody and from 2342 to 3118 for polyclonal antibody (78/dec for the monoclonal antibody and 58/dec for polyclonal antibody), which were translated directly from the drain waveform into the digital readout using the architecture previously stated. Note that the sensor has not reached saturation for up to $10\ \mu\text{g/ml}$ in concentration, showing the wide applicability in such a sensor system; however, a higher testing concentration than that in this work that might saturate the sensor response is not relevant in actual clinical sample detection.

Compared with conventional nasal (anterior nares, midturbinate, and nasopharyngeal) and oropharyngeal specimens, which require preparation of test samples in a viral transport medium (VTM), advances in sensing technology using saliva samples offer a unique advantage in a painless and facile sample collection process, which shows the promise of electrical testing compared

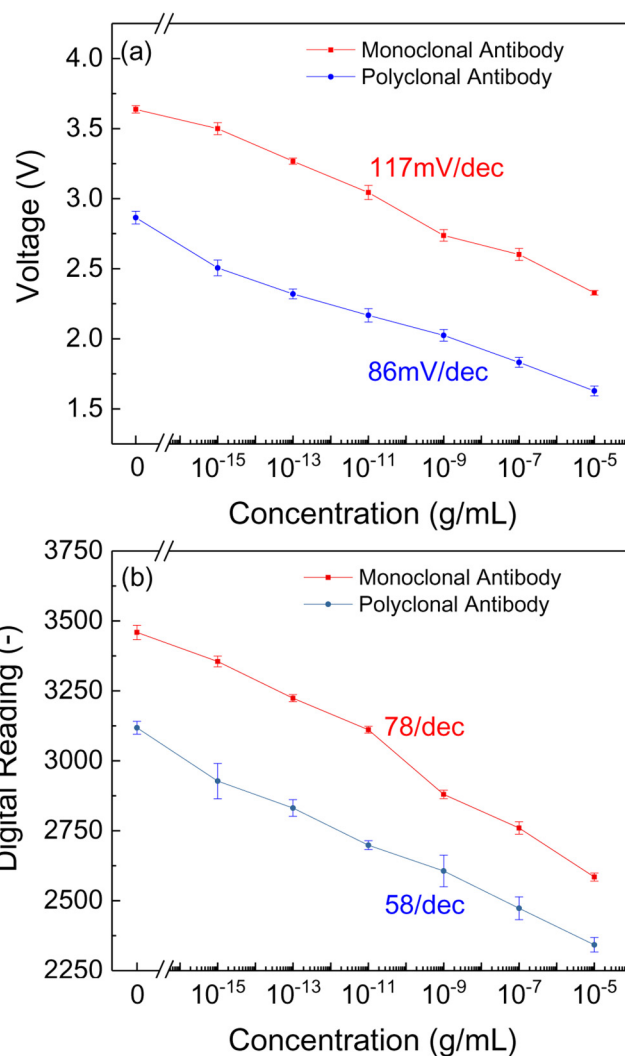


FIG. 5. Average voltage reading extracted at $750\ \mu\text{s}$ from a drain waveform for different concentrations of a SARS-CoV-2 spike peptide in artificial saliva (a) and average digital reading (b) using a test strip functionalized with a SARS-CoV-Spike monoclonal antibody and polyclonal spike antibody.

with the traditional PCR method in testing human saliva. Given the high sensitivity down to 1 fg/ml of the spiked protein and low relative standard deviation (maximum 1.7 % at 100 ng/ml for the monoclonal antibody and 2.2 % at 10 pg/ml for polyclonal antibody), the application of our current measurement system was further evaluated using inactivated human virus in artificial saliva as the medium.

Human-inactivated virus (ATCC VR-1986HK) was purchased from a vendor and was serially diluted into various concentrations from 100 to 2500 plaque forming units per milliliter (PFU/ml). The response curves for both analog and digital data throughout the concentration range are shown in Fig. 6. Interpolations from

the concentration range in Fig. 6(a) show sensitivities of 465 mV/dec for the monoclonal antibody and 649 mV/dec for polyclonal antibody tested. Likewise, Fig. 6(b) shows similar changes in the digital readout range compared with spiked peptide, with a calculated sensitivity in a digital reading of 356/dec for the monoclonal antibody and 454/dec for its polyclonal counterpart. The higher sensitivity of the polyclonal antibody in this case shows great promise for future investigations into extending to lower limits of detection.

The choices between polyclonal and monoclonal antibodies depend on many factors. Polyclonal antibodies are more readily

available, are less expensive, and are highly stable with high affinity. By contrast, monoclonal antibodies have the advantage of homogeneity and consistency.^{35,36} When tested with protein, the polyclonal and monoclonal antibodies showed relatively similar sensitivity. When it came to virus detection, polyclonal antibodies showed slightly stronger signals than monoclonal antibodies. This is probably because polyclonal antibodies can recognize different epitopes of the target molecule, so that binding to different epitopes from one target virus is likely. The tighter binding could strengthen the detection signals. However, because of the polyclonal antibodies' tolerance to the minor difference between antigens, and the fact of

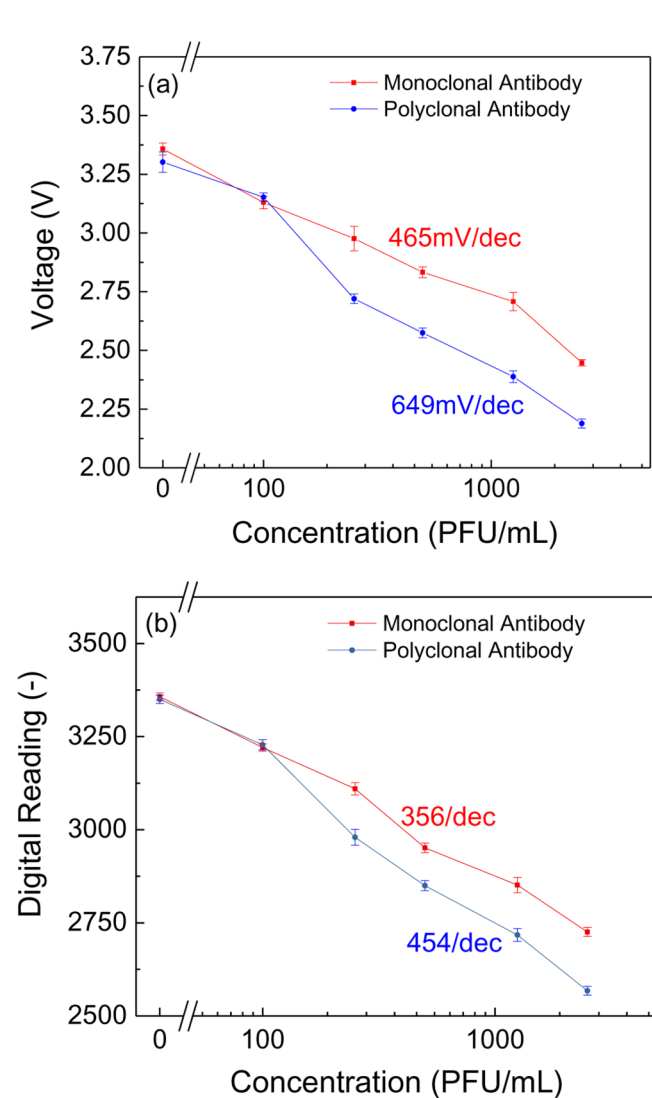


FIG. 6. Average voltage reading extracted at 750 μ s from a drain waveform for different concentrations of inactivated virus (ATCC VR-1986HK) in artificial saliva (a) and average digital reading (b) using a test strip functionalized with a SARS-CoV-Spike monoclonal antibody and polyclonal spike antibody.

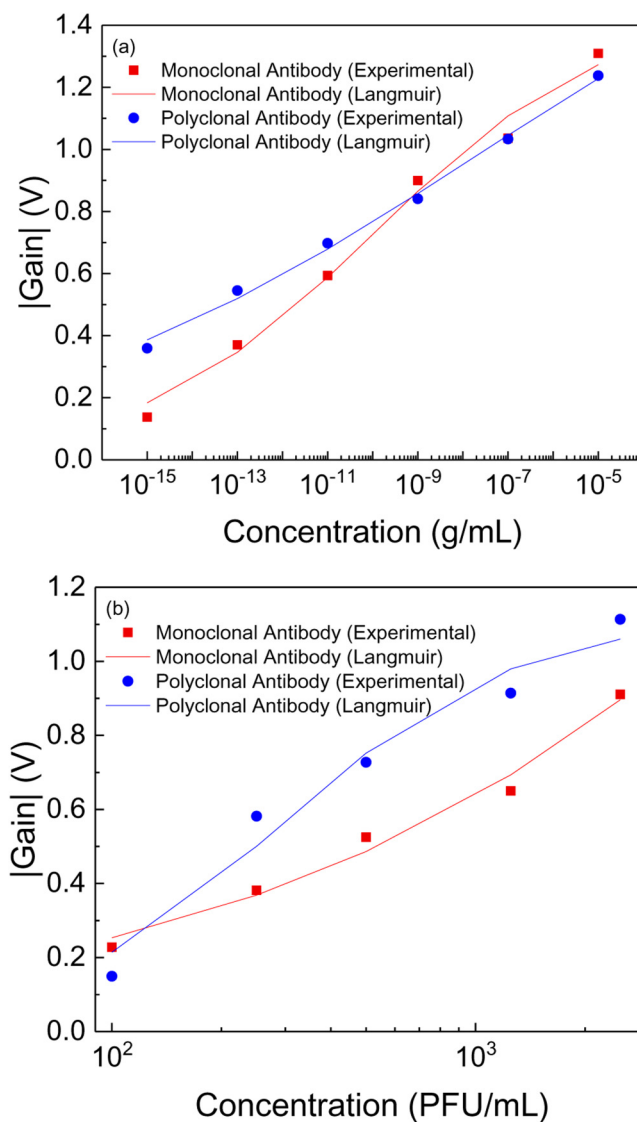


FIG. 7. Net drain voltage changes for a sensor strip exposed to different spiked protein (a) and inactivated virus (b) concentrations and model fitting by the Langmuir extension model.

their being affected more by background noise and cross-reactivity, the use of polyclonal antibodies might lead to an increased possibility of false-positive results for pathogen screen testing.³⁷

Yang *et al.* previously reported that the reversible binding process of antigen–antibody complexes can be modeled by the Langmuir extended isotherm, correlating the gain of the sensor as a function of antigen concentration,^{28,38}

$$|\Delta V| = \frac{q_m b [c]^\eta}{1 + b [c]^\eta},$$

where q_m and b are constants, $[c]$ is the tested antigen concentration, and η is related to the spread of energy distribution.^{38,39}

Figure 7 shows good fitting for both sets of data for the S protein and virus via fitting the net change of drain voltage versus sample concentration using the Langmuir extended isotherm, showing the small molecule approximation is still valid in the tested range we examined.

CONCLUSION

The ongoing SARS-CoV-2 pandemic has made rapid and decentralized PCR and serology testing technology essential. The portable and inexpensive cartridge sensor system described here provides the opportunity for off-site biomarker testing of viral and life-threatening diseases with fast turnaround time. This study presents a modular sensor system with a disposable sensor strip made with Au-plated and biofunctionalized electrodes, specifically for the detection of COVID-19. Two different commercially available antibodies were successfully tested, with a limit of detection down to 1 fg/ml for a spike peptide and 100 PFU/ml for an inactivated virus. This shows the potential for point-of-care COVID-19 detection with high sensitivity using a biosensor system based on a semiconductor transistor.

ACKNOWLEDGEMENTS

The work at UF is partially supported by the National Institute of Dental and Craniofacial Research (NIDCR) at The National Institutes of Health (NIH) under Grant No. R01-DE025001.

DATA AVAILABILITY

The data that support the findings of this study are available from the corresponding author upon reasonable request.

REFERENCES

- ¹M. Lotfi, M. R. Hamblin, and N. Rezaei, *Clin. Chim. Acta* **508**, 254 (2020).
- ²World Health Organization, WHO Coronavirus (COVID-19) Dashboard, 2021.
- ³B. Udugama *et al.*, *ACS Nano* **14**, 3822 (2020).
- ⁴L. Azzi *et al.*, *J. Infect.* **81**, e45 (2020).
- ⁵A. La Marca, M. Capuzzo, T. Paglia, L. Roli, T. Trenti, and S. M. Nelson, *Reprod. BioMed. Online* **41**, 483 (2020).
- ⁶Y. W. Tang, J. E. Schmitz, D. H. Persing, and C. W. Stratton, *J. Clin. Microbiol.* **58**, e00512 (2020).

- ⁷R. Lu *et al.*, *Lancet* **395**, 565 (2020).
- ⁸G. Seo *et al.*, *ACS Nano* **14**, 5135 (2020).
- ⁹P. Ranjan, A. Singhal, S. Yadav, N. Kumar, S. Murali, S. K. Sanghi, and R. Khan, *Int. Rev. Immunol.* **40**, 126 (2021).
- ¹⁰M. Xian, P. H. Carey, C. Fares, F. Ren, S. S. Shan, Y. Te Liao, J. F. Esquivel-Upshaw, and S. J. Pearton, *IEEE Research and Applications of Photonics in Defense Conference, RAPID 2020—Proceedings*, virtual conference, 10–12 August 2020 (IEEE, New York, 2020).
- ¹¹J. Zhao *et al.*, *Clin. Infect. Dis.* **71**, 2027 (2020).
- ¹²M. Z. Rashed, J. A. Kopechek, M. C. Priddy, K. T. Hamorsky, K. E. Palmer, N. Mittal, J. Valdez, J. Flynn, and S. J. Williams, *Biosens. Bioelectron.* **171**, 112709 (2021).
- ¹³R. Sabino-Silva, A. C. G. Jardim, and W. L. Siqueira, *Clin. Oral Invest.* **24**, 1619 (2020).
- ¹⁴A. L. Wyllie *et al.*, *N. Engl. J. Med.* **383**, 1283 (2020).
- ¹⁵E. Williams, K. Bond, B. Zhang, M. Putland, and D. A. Williamson, *J. Clin. Microbiol.* **58**, e00776 (2020).
- ¹⁶J. Xu, Y. Li, F. Gan, Y. Du, and Y. Yao, *J. Dent. Res.* **99**, 989 (2020).
- ¹⁷Y. Li, B. Ren, X. Peng, T. Hu, J. Li, T. Gong, B. Tang, X. Xu, and X. Zhou, *Mol. Oral Microbiol.* **35**, 141 (2020).
- ¹⁸D. Sapkota *et al.*, *J. Clin. Pathol.* **0**, 206834 (2020).
- ¹⁹P. Han and S. Ivanovski, *Diagnostics* **10**, 290 (2020).
- ²⁰E. Pasomsub, S. P. Watcharananan, K. Boonyawat, P. Janchompoo, G. Wongtabtim, W. Sukswan, S. Sungkanuparph, and A. Phuphuakrat, *Clin. Microbiol. Infect.* **27**, 285.e1 (2021).
- ²¹M. Alafeef, K. Dighe, P. Moitra, and D. Pan, *ACS Nano* **14**, 17028 (2020).
- ²²B. S. Kang *et al.*, *Appl. Phys. Lett.* **89**, 122102 (2006).
- ²³B. S. Kang, F. Ren, M. C. Kang, C. Lofton, W. Tan, S. J. Pearton, A. Dabiran, A. Osinsky, and P. P. Chow, *Appl. Phys. Lett.* **86**, 112105 (2005).
- ²⁴T. J. Anderson, K. D. Hobart, M. J. Tadjer, A. D. Koehler, T. I. Feygelson, B. B. Pate, J. K. Hite, F. J. Kub, and C. R. Eddy, *ECS Trans.* **64**, 185 (2014).
- ²⁵R. Mehandru, B. Luo, B. S. Kang, J. Kim, F. Ren, S. J. Pearton, C. C. Pan, G. T. Chen, and J. I. Chyi, *Solid-State Electron.* **48**, 351 (2004).
- ²⁶B. S. Kang, F. Ren, B. P. Gila, C. R. Abernathy, and S. J. Pearton, *Appl. Phys. Lett.* **84**, 1123 (2004).
- ²⁷P. H. Carey *et al.*, *J. Electrochem. Soc.* **167**, 037507 (2020).
- ²⁸J. Yang, P. Carey, F. Ren, M. A. Mastro, K. Beers, S. J. Pearton, and I. I. Kravchenko, *Appl. Phys. Lett.* **113**, 032101 (2018).
- ²⁹J. Yang, P. Carey, F. Ren, Y. L. Wang, M. L. Good, S. Jang, M. A. Mastro, and S. J. Pearton, *Appl. Phys. Lett.* **111**, 202104 (2017).
- ³⁰S.-S. Shan *et al.*, *IEEE Trans. Biomed. Circuits Syst.* **14**, 1362 (2020).
- ³¹S. Y. Lu, S. S. Shan, J. Yang, C. W. Chang, F. Ren, J. Lin, S. Pearton, and Y. Te Liao, *Proceedings of Annual International Conference of the IEEE Engineering in Medicine and Biology Society EMBS*, Berlin, Germany, 23–27 July 2019 (IEEE, New York, 2019), pp. 5761–5764.
- ³²Y. Xue, X. Li, H. Li, and W. Zhang, *Nat. Commun.* **5**, 5357 (2014).
- ³³X. Wu, W. Tang, C. Hou, C. Zhang, and N. Zhu, *Microchim. Acta* **181**, 991 (2014).
- ³⁴J. Chen, A. F. Zheng, A. H. Chen, Y. Gao, C. He, X. Kai, G. Wu, and Y. Chen, *Anal. Chim. Acta* **599**, 134 (2007).
- ³⁵N. S. Lipman, L. R. Jackson, L. J. Trudel, and F. Weis-Garcia, *ILAR J.* **46**, 258 (2005).
- ³⁶B. Byrne, E. Stack, N. Gilmartin, and R. O’Kennedy, *Sensors* **9**, 4407 (2009).
- ³⁷P. Nina, S. Mark, T. T. Anh-Hue, L. Philip, and B. M. Forster, *Microbiology* (OpenStax, Houston, TX, 2016).
- ³⁸A. Kapoor, J. A. Ritter, and R. T. Yang, *Langmuir* **6**, 660 (1990).
- ³⁹P. H. Carey, J. Yang, F. Ren, C.-W. Chang, J. Lin, S. J. Pearton, B. Lobo, and M. E. Leon, *J. Electrochem. Soc.* **166**, B708 (2019).